Research Article

Investigation on the Aerodynamic Parameters of the Triangle Shape of Tall Buildings by Using of CFD Method

Mehdi Noormohamadian [ID] **and Eysa Salajegheh**

Department of Civil Engineering, Shahid Bahonar University of Kerman, Kerman, Iran

Correspondence should be addressed to Mehdi Noormohamadian; mehdi.noormohamadian@eng.uk.ac.ir

Wind loading in large buildings has always been a major challenge for civilian engineers. For this purpose, presenting the optimum exterior forms of a building exposed to the wind flow and analyzing aerodynamic forces, including resistance force, bending, and twisting moments, are challenging issues for designers. Nowadays, by combining various numerical calculation methods, like neural networks, genetic algorithms, and other methods, by changing some parameters, they optimize the external form of the building based on aerodynamic parameters. In this research, three optimized triangular models will be investigated using the computational fluid dynamics method. For wind flow, a velocity profile is used in the three simulations, and Reynolds' Navier–Stokes average equations are used to solve momentum relationships. Additionally, the κ-ε method was used to calculate Reynolds stresses. The results show that the optimized N3 model is in the most optimal condition possible in terms of aerodynamic parameters such as drag, torsion moment, and vortices behind the building. Nowadays, the neural network algorithm is one of the most famous numerical methods for optimizing hull shapes. However, this approach cannot improve aerodynamic parameters either. Hence, computational fluid dynamics is used to deeply analyze. This research is one step forward to assess the optimized hull shapes of tall buildings. All tests are conducted using STAR CCM+.

1. Introduction

The focus on tall buildings is not recent and began in the late 19th century in the United States—the Monadnock Building in Chicago was built in 1891 and was one of the first 15-story skyscrapers [1]. The construction of tall buildings has been in response to economic needs, due to the ever-increasing population and economic activities [2].

In addition, in the field of environmentally friendly construction, tall buildings are considered a sustainable choice because they help to focus activities by providing large office and residential spaces in a limited place and can help limit urban expansion [3].

It is well established that structural form plays an important role in wind resistance and structural response in both directions. Bluff structures are more exposed to high wind loads [4]. Previous records of such studies can be found in the studies of Lee and Hershberger [5], Irwin [4]. Rectangular cross-sections are more susceptible to lateral response than triangular, elliptical, and cylindrical forms [5]. These shapes have greater structural effectiveness. Today, even if the safety of the structure can be confirmed by using advanced systems and high-quality materials, still the vibrations caused by the wind can be beyond the human comfort zone and may cause fatigue during the life of the building, excessive noise, and cracks [6]. The dynamic movement of the building depends on factors such as the characteristics of the wind flow, the surrounding environment of the building, the shape and height, and the structural characteristics of the building (that is, stiffness, damping, mass distribution, mode shape, etc.). This secondary parameter is considered important because this motion is perceived by residents and can cause discomfort or disturbance to residents [7]. Therefore, the field of wind load and response reduction has always been a critical, interesting, and researchable field among researchers and has been continuously paid attention to [8].
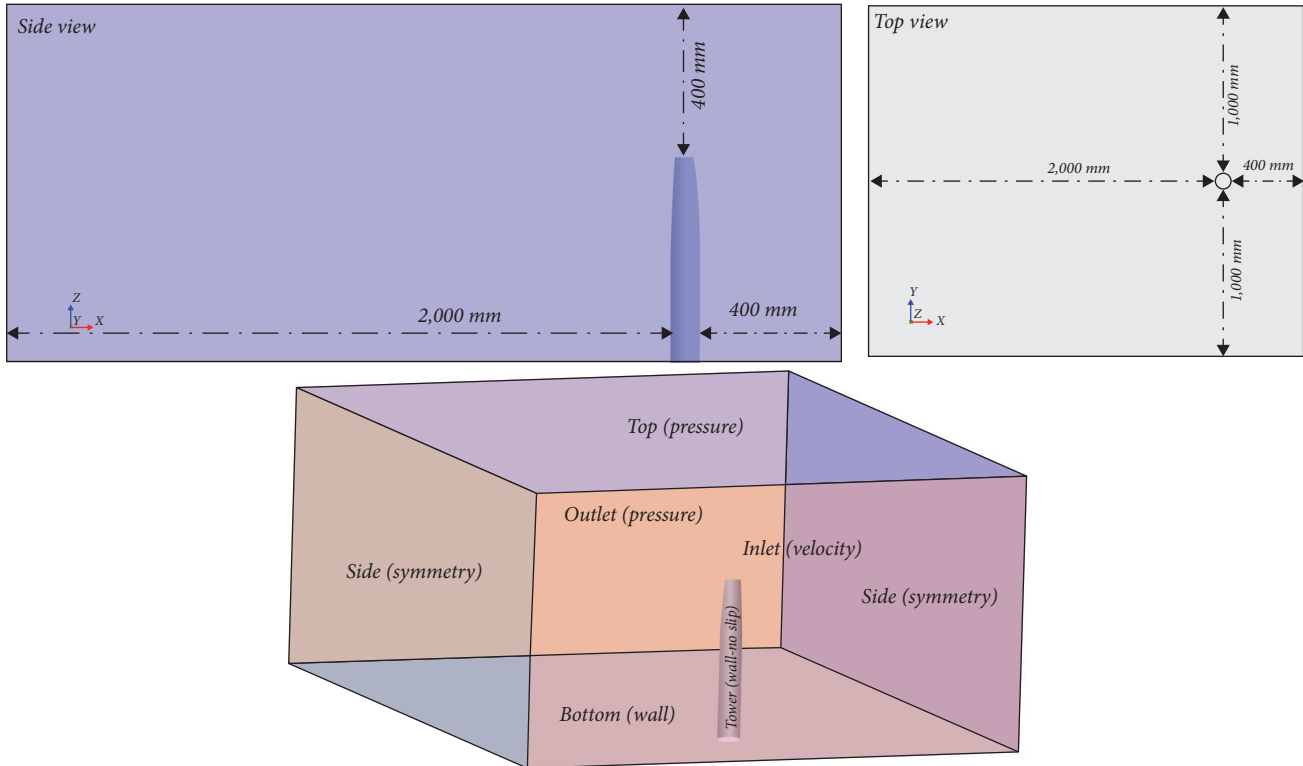
FIGURE 1: Dimensions of the computational domain and boundary conditions.

In order to be able to form the external shape of the building in such a way that it has a suitable aerodynamic performance, an optimization process should be considered to minimize the aerodynamic responses in this process [9]. In this process, the effect of all aerodynamic modifications can be observed. Because both wind directions exert significant responses on the tall building, it is necessary to apply the effect of both directions simultaneously; therefore, the non-dominated sorting genetic algorithm (NSGAII) multiobjective optimization method is used in this study. To this end, the exterior shape of the building should be set and the effect of each parameter on the aerodynamic response should be checked. There are different methods for parameterization, in this study, the polynomial method was used. The computational fluid dynamics (CFD) numerical method has been used to calculate the aerodynamic response, and a new building model must be produced and analyzed in each iteration of the optimization process, which is time-consuming, so we need an alternative method instead of the time-consuming CFD analysis.

The positions of the two control points (design variables) are used to determine the shape of the spline curve as the corner shape of a square section. The objective function can be estimated within each Aspect-Oriented Programming iteration process by CFD analysis. Because this analysis involves a high calculation cost, it is necessary to use another model. In the research done by Bernardini et al. [10] the Kriging model was used as an alternative model to evaluate the drag and lift coefficient (objective functions). Elshaer et al.

[11] achieved the optimal ear shape of a square section based on two design variables and investigated different kinds of angle corrections. They used the alternative model to evaluate the objective function in each iteration process and confirmed that the alternative model could contribute to an acceptable saving of computation time. The findings showed that the artificial neural networks (ANN) model correctly obtains 1, resulting in a training model/database, and the effective ANN correlation coefficient of 979 for the mine is the aerodynamic responses of the building.

The aim was used to compare the aerodynamic performance of different models. These functions were optimized in a bi-objective optimization process using NSGAII. The obtained results show the accuracy of the proposed method to increase the aerodynamic performance of tall 3D buildings [12]. A polynomial method is used for shape parameterization to construct the outer shape of buildings. The proposed method can investigate different aerodynamic changes in the exterior of a tall building with a triangular cross-section using seven geometric parameters.

Previously, a number of researchers recognized that the dynamic response of the crosswind might exceed the response along the wind [13–15], and movement in the transverse direction can be a serious issue not only for structural fatigue but also for serviceability design as shown in Figure 1(b). A vortex appears that gives the root mean square value for the transverse direction greater than the longitudinal direction of the wind. Irwin et al. [16] reported that the responses of the Jin Mao building showed approximately two transverse

directions relative to the downwind direction. Although vortex shedding is the main driving mechanism that affects the crosswind motion, the knocking phenomenon is driven by the turbulence of the upstream building. It is also responsible and may inhibit the stimulation [16].

Rigidity is considered a significant aspect of structural stability and response. High wind speed and low stiffness make the structure more prone to the vortex created by transverse wind vibrations [17]. It has been proven that increasing the stiffness of the building (which increases the natural frequency of the building) By choosing a suitable structural system, it is one of the most efficient methods to suppress the movement of the structure without affecting the exterior of the structure [7, 15]. It can be inappropriate and may lead to an increase in the cost invested in the construction, and in addition, it can reduce the usable surface inside (because the size of the columns has to be increased).

Kim and Kanda [18] found a successful reduction in the downwind overturning moment and crosswind yawing moment for the cone and retreat model (retreat at average height and same surface area). In another study by Kim and Kand [19] reported for similar models that the average along the wind and the fluctuation of wind forces can be greatly reduced to increase the taper ratios, but the lag model is more valuable than the taper models. Kim and Kand [19] reported through a collection of wind pressure measurements on conical and receding models that the pressure on the windward faces does not change significantly, but due to the change in the geometrical characteristics, the minimum absolute value of the pressure coefficient It is bigger than the square model. Due to the change in width along the height, the frequency of shedding changes, and the formation of eddies changes upward [19].

Noormohamadian and Salajaghe [20] optimized drag and lift force and torque for a large triangular tower using the genetic algorithm. They can reduce the drag and lift coefficient by 62% and 93%. Moreover, they (2022) can introduce an equation for the optimization of triangular towers by connecting the CFD method to the ODE solver. They reached 56% optimization of the drag coefficient. In this research, certainly, three optimized models of Noormohamadian and Salajaghe's [20] research will be compared based on the aerodynamic parameters. So, in this research, vortices, velocity, and pressure around each of the three models will be compared, and also, the distribution of shear stress and pressure and consequently, pressure, shear, and total drag will be presented. In the end, an optimized model based on the aerodynamic approach will be introduced to this goal, and the CFD method as a good instrument has been used. All tests are running by using STAR CCM+.

2. Governing Equation

The basis of computational fluid dynamics is the fundamental equation of fluid dynamics. These equations provide a mathematical model to describe viscous Newtonian flows. The complete governing fluid equations were first presented by the French scientist Navier in 1822 and independently by the English scientist Stokes in 1845. These equations are second-order nonlinear partial differential equations and are very difficult to solve. There is little hope to achieve the exact solution of these equations in the general case, but for some special cases, such as specific flows with simple boundaries, the analytical solution of the Navier–Stokes equations has been made possible, and its results are also used in some engineering applications.

2.1. Equation of Conservation of Mass. The equation of conservation of mass, which is often named the continuity relation, is of fundamental importance and will be true in all flow fields regardless of what simplifying assumptions are considered. This law states that the total time rate of mass change per unit volume is zero. The compact form of the continuity equation is as follows:

$$\frac{\partial \rho}{\partial t} + \frac{\partial(\rho u_i)}{\partial x_i} = 0. \tag{1}$$

If the fluid is assumed to be compressible, the continuity equation is expressed as Equation (2):

$$\frac{\partial u_i}{\partial x_i} = \frac{\partial u}{\partial x} + \frac{\partial v}{\partial y} + \frac{\partial w}{\partial z} = 0. \tag{2}$$

2.2. Conservation Equation of Linear Motion. The relationship between the stress field and the deformation of the field due to the spatial and temporal change of speed expresses the law of conservation of momentum. Navier–Stokes equations express the constancy of the movement size in mathematical terms and are written as a relation for compressible flow as follows:

$$\frac{\partial(\rho u_i)}{\partial t} + \frac{\partial}{\partial x_j}\left(\rho u_i u_j\right) = -\frac{\partial p}{\partial x_i} + \frac{\partial}{\partial x_j}\left[\mu\left(\frac{\partial u_i}{\partial x_j} + \frac{\partial u_j}{\partial x_i}\right)\right] + \rho g_i. \tag{3}$$

If the flow is incompressible and has constant properties, this equation can be written as Equation (4):

$$\rho\frac{\partial u_i}{\partial t} + \rho\frac{\partial}{\partial x_j}\left(u_i u_j\right) = -\frac{\partial p}{\partial x_i} + \mu\nabla^2 u_i + \rho g_i. \tag{4}$$

2.3. Turbulence. To model the fluid flow, the full solution of the equations is required, and on the other hand, the upcoming problem is a turbulent flow due to the high Reynolds number. In most flows with high Reynolds, the effect of viscous forces is limited to the region near the wall, which is called the boundary layer. The boundary layer starts from a set of regular streamlines in which the fluid oscillates at the microscopic level. Such a boundary layer is called a relaxed boundary layer. Gradually and due to the conditions caused by

the geometrical shape and flow fields, such as surface roughness and pressure gradient, the fluid fluctuation increases to the microscopic level, and the flow lines no longer remain regular, in which case the smooth flow turns into a turbulent flow. One of the characteristics of turbulent flow is the fluctuations in the velocity field. Because these oscillations occur on a very small scale and with very high frequencies, it is impossible to model them directly in most engineering applications. Of course, in theoretical applications, for very simple geometries and at low Reynolds numbers, by solving the original form of the Navier–Stokes equation, these fluctuations can be directly modeled, albeit on a small scale and high frequency, which, of course, entails a relatively high computational cost.

In flows with high Reynolds, average values of velocity, pressure, shear stress, etc., are more important to engineers. This kind of attitude led Reynolds in 1895 to write the equations governing the flow in terms of mean or time average variables of turbulent flow. The basis of the method that Reynolds used to study turbulence was based on this method, which replaces the values of velocity and pressure or any other quantity such as φ as the sum of average values and instantaneous fluctuations ($\varphi = \acute{\varphi} + \overline{\varphi}$) in the Navier–Stokes equation. And then averaged the entire equation concerning time; the resulting equation was the Reynolds equation, which is the so-called Reynolds' Navier–Stokes (RANS) equation. This equation is expressed in Cartesian coordinates as Equation (5):

$$\frac{\partial(\rho\overline{u_i})}{\partial t} + \frac{\partial}{\partial x_j}\left(\rho\overline{u_i u_j}\right)$$
$$= -\frac{\partial\overline{p}}{\partial x_i} + \frac{\partial}{\partial x_j}\left[\mu\left(\frac{\partial\overline{u_l}}{\partial x_j} + \frac{\partial\overline{u_j}}{\partial x_i}\right) - \rho\overline{\acute{u}_l\acute{u}_j}\right] + \rho g_i. \tag{5}$$

These equations do not form a closed system, and the number of unknowns is more than the number of equations. Due to the nonlinearity of these equations, after the averaging process, the correlation between the velocity fluctuations $\rho\overline{\acute{u}_l\acute{u}_J}$ is raised, which is called Reynolds stress or disturbance stress. Therefore, it is necessary to either define additional equations or reduce the number of unknowns in some way. To solve this problem, Bozisenko defined the Reynolds stress as a function of the velocity gradient and μ_t, the relationship of which is as follows:

$$-\rho\overline{\acute{u}_l\acute{u}_J} = \mu_t \frac{\partial\overline{u_i}}{\partial j x_j}. \tag{6}$$

The purpose of turbulence models is to relate the size of these turbulent stresses to the mean velocity field. So far, many turbulence simulators have been introduced, which are reliable in simulating special flow regimes in a unique flow field. The ultimate goal of all turbulence models is to calculate the size of the Reynolds stresses. In the following, two turbulence models that are used in marine problems are introduced:

2.3.1. κ-ε Model. The κ-ε model is one of the most famous and powerful two-equation models for solving turbulent flow in engineering problems because solving the two transport equations separately allows the turbulence velocity and characteristic length to be determined separately. This model is a semiempirical model, and its equations are based on experimental observations. In this model, κ is the kinetic energy of turbulent flow and is the turbulent kinetic energy loss rate, and Equation (7) is used to calculate the turbulence viscosity:

$$\mu_t = C_\mu\rho\frac{K^2}{\varepsilon}, \tag{7}$$

where C_μ is an empirical coefficient, whose value is usually considered to be 0.09, and semiempirical Equations (8) and (9) are used to calculate κ and ε:

$$\frac{\partial(\rho k)}{\partial t} + \frac{\partial}{\partial x_i}(\rho k u_i) = \frac{\partial}{\partial x_j}\left[\left(\mu + \frac{\mu_t}{\partial_k}\right)\frac{\partial_k}{\partial x_j}\right] + G_k - Y_m - \rho\varepsilon, \tag{8}$$

$$\frac{\partial(\rho k)}{\partial t} + \frac{\partial}{\partial x_i}(\rho\varepsilon u_i) = \frac{\partial}{\partial x_i}\left[\left(\mu + \frac{\mu_t}{\sigma_\varepsilon}\right)\frac{\partial_\varepsilon}{\partial x_i}\right] + C_{1\varepsilon}\frac{\varepsilon}{k}G_k - C_{2\varepsilon}\rho\frac{\varepsilon^2}{k}, \tag{9}$$

where $C_{1\varepsilon}$ and $C_{2\varepsilon}$ are empirical coefficients, and σ_κ and σ_ε are chaotic according to Pyrantel and Schmidt numbers. The terms $C_{1\varepsilon}\frac{\varepsilon}{\kappa}G_\kappa$ and $C_{2\varepsilon}\rho\frac{\varepsilon^2}{\kappa}$ in the equation represent the shear stress production processes ε and vicious loss ε, respectively.

The term G_κ expresses the amount of kinetic energy production of turbulence caused by the turbulent flow field and its effects on the average flow, which is called the shear production term as follows:

$$G_k = -\rho\overline{\acute{u}_l\acute{u}_J}\frac{\partial u_i}{\partial x_j}. \tag{10}$$

The Y_m term also represents the contribution of fluctuating expansion to the rate of total dissipation of turbulence in compressible flow. The oscillatory expansion represents the damping of the turbulence energy caused by the compressibility of the fluid. Since the compressible fluid is assumed in this problem, this term does not affect existing calculations.

$$Y_m = 2\rho\varepsilon\frac{k}{\gamma^{RT}}. \tag{11}$$

For isothermal flow without mass transfer, the optimized coefficients are the following.

3. Model Description and Physics

In this research, three optimized models of Noormahamadian and Salajaghe [20] named N1, N2, and N3 are used; the

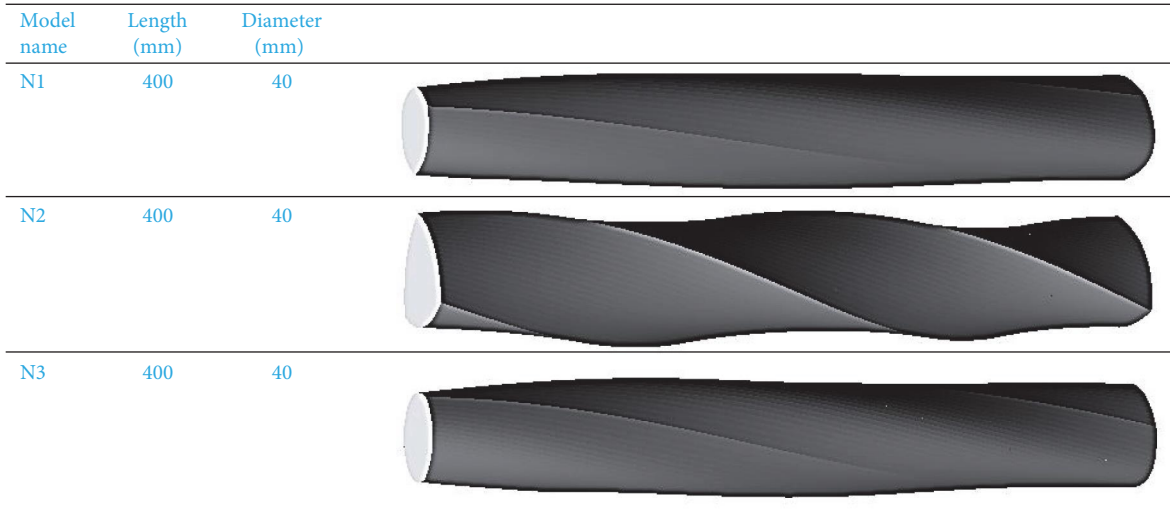| Model name	Length (mm)	Diameter (mm)	
N1	400	40	
N2	400	40	
N3	400	40	

FIGURE 2: View of three optimized models based on the work of Noormahamadian and Salajaghe [20].

height is 400 mm and the diameter for all models is 40 mm. These models were optimized based on the aerodynamic parameters and resulted in the neural network algorithm. In Figure 2(a), a view of all three models is presented.

Dimension of domain and boundary conditions are two effective parameters on the result of the numerical methods. These are affected by reversed flow at the outlet boundary, wake around the building and the flow at the top of the building. So, dimensions and boundary conditions are selected in Figure 1.

In this research, the speed profile is defined based on Equation (12) in terms of height from the ground:

$$U(z) = U_h \left(\frac{z}{H}\right)^a, \tag{12}$$

where U_h is the wind speed at the top of the tower, H is the tower height and a is 027. Also, turbulence intensity is defined based on Equation (13):

$$I(z) = 0.1 \left(\frac{z}{H}\right)^{(-a-0.05)}. \tag{13}$$

Velocity profile and turbulence intensity according to height in Figure 3 it has been shown.

The steady model is utilized for all steady-state simulations. There are two models available in Simcenter STAR-CCM+ to calculate the wall distance (STAR CCM+, 2021):

(i) Exact wall distance.

(ii) PDE wall distance.

The accurate wall spacing model performs an accurate prediction calculation in real space based on triangulation of the surface grid. The application of K_d search trees or Implicit Tree methods accelerates the calculation. In this simulation, exact wall distance has been used for calculating wall distance. Another physics that is applied in this simulation is the segregated flow model that invokes the segregated

solver, which solves each of the momentum equations, in turn, one for each dimension.

4. Mesh Study

One of the most important influencing factors in numerical analysis is the type of meshing of the solution domain. The trimmer mesh technique is also used in this research for gridding the solution domain. The corrected cell masher provides a strong method for creating a qualified mesh for both simple and comprehensive mesh generation problems. It merges several meshing properties in a single meshing scheme that is predominantly hexahedral mesh upon surface mesh and independence alignment.

Due to a lack of laboratory test results, the only way to confirm the numerical results was to check the convergence of the results in different meshes. For this purpose, the total drag coefficients of all three models in five different meshing modes, which were compared with each other, and the results are based on Figure 4 obtained. Figure 5 shows a view of the fine meshing by trimming mesh, which is 1,869,563 meshes used in this research.

5. Results

The results of the simulation will be shown after a verification process. Figure 6 shows the pressure contour around the model in Section 4 heights of 0.1, 0.2, 0.3, and 0.4 m from the ground surface.

According to Figure 6, pressure is between −40 and 40 Pa. The surface in front of the air for N2 is less than the two others, and the result is more pressure. Also, the drop pressure around the hull in N2 model is less than in two other models. Figure 7 shows the vorticity around X axis for four section plane which is perpendicular of Z axis.

Based on Figure 7, the separation of the airflow in N3 and N1 occurs later than in the N2 model, and this phenomenon has more eddy pressure consequences. Another important
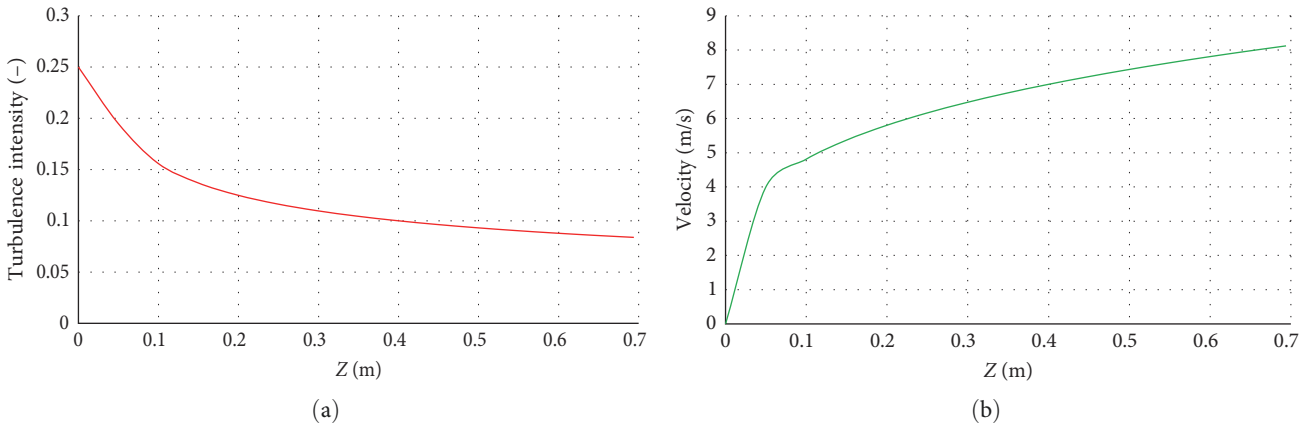
(a)

(b)

FIGURE 3: Changes in (a) turbulence intensity and (b) velocity depending on the height above the ground.
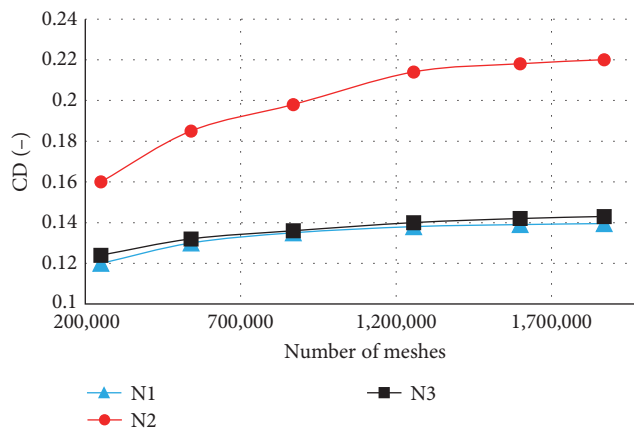

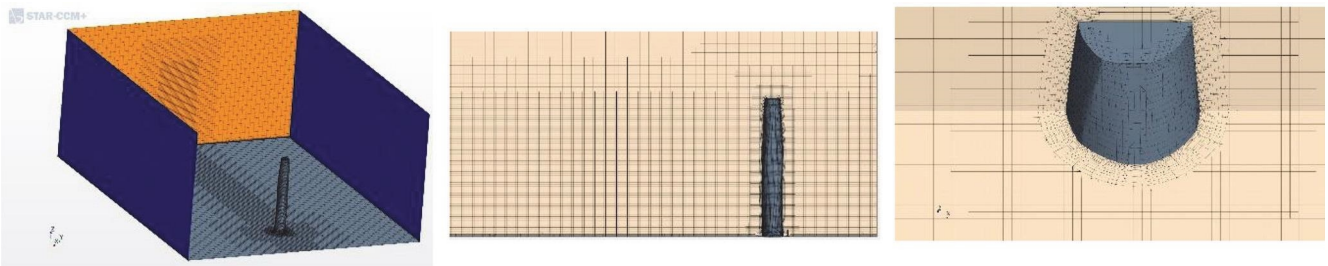FIGURE 4: Comparison of C_d for three models in different mesh grids.

FIGURE 5: A different view of the fine mesh grids.

result is about N3 in comparison of N1, where the separation of the airflow happens later.

Figure 8 shows the velocity magnitude around the three models for four plane section perpendicular Z axis.

As shown in Figure 8, the middle of the N2 wake is so greater than the two other models, which makes greater viscous-pressure force. It can increase the pressure drag extremely. Also, the wake of the N3 back tower is less than the N1 model.

Another parameter present in this research is Q-Criterion which shows the 3D vortex around the model. The equation for Q-Criterion is based on Equation (14).

$$Q - \text{Criterion} = 0.5 \left(\text{vorticity}^2 - \text{strain rate}^2 \right). \qquad (14)$$

The value for the Q-Criterion for all three models is 500 $1/s^2$. Figure 9 shows the Q-Criterion parameter for the three models.
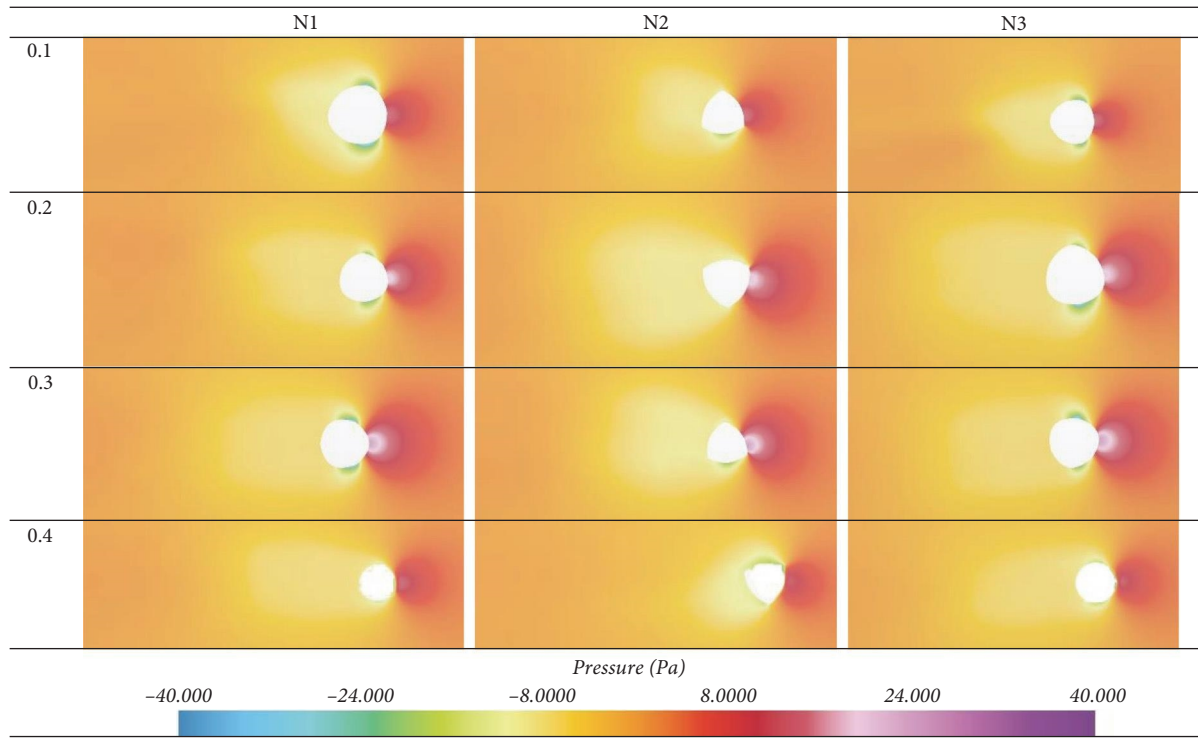
FIGURE 6: Pressure distribution around the model from top view for three models and four different heights from ground bed.
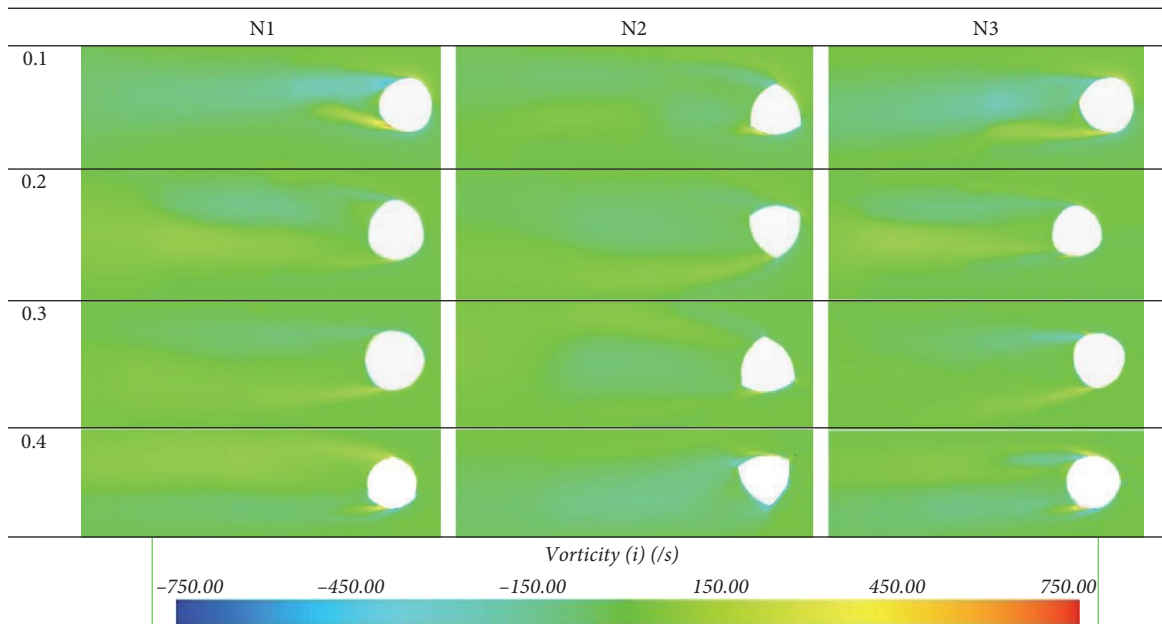

FIGURE 7: Vorticity about the X axis around the model from top view for three models and four different heights from ground bed.

Figure 9 shows that the vorticity around the N2 model at the middle is greater than the two others; also, flow separation occurred sooner at N2 model, and consequently, viscous pressure is greater than the two others.

In this research, the most important result is pressure, shear and total resistance, Y-axis force, Z, Y-axis moment, and area in touch with air, which is calculated based on

Table 1. Also, Table 2 shows the nondimensional results. The green color shows the least value among the three models. In Table 1, R_s is frictional forces, R_p is pressure force, R_t is total force, M_y is moment around Y axis, M_z is moment around Z axis, and A is the area in face of the wind. Also, in Table 2, C_F is frictional force coefficient, C_P is pressure force coefficient, C_t is total force coefficient C_{My} is moment
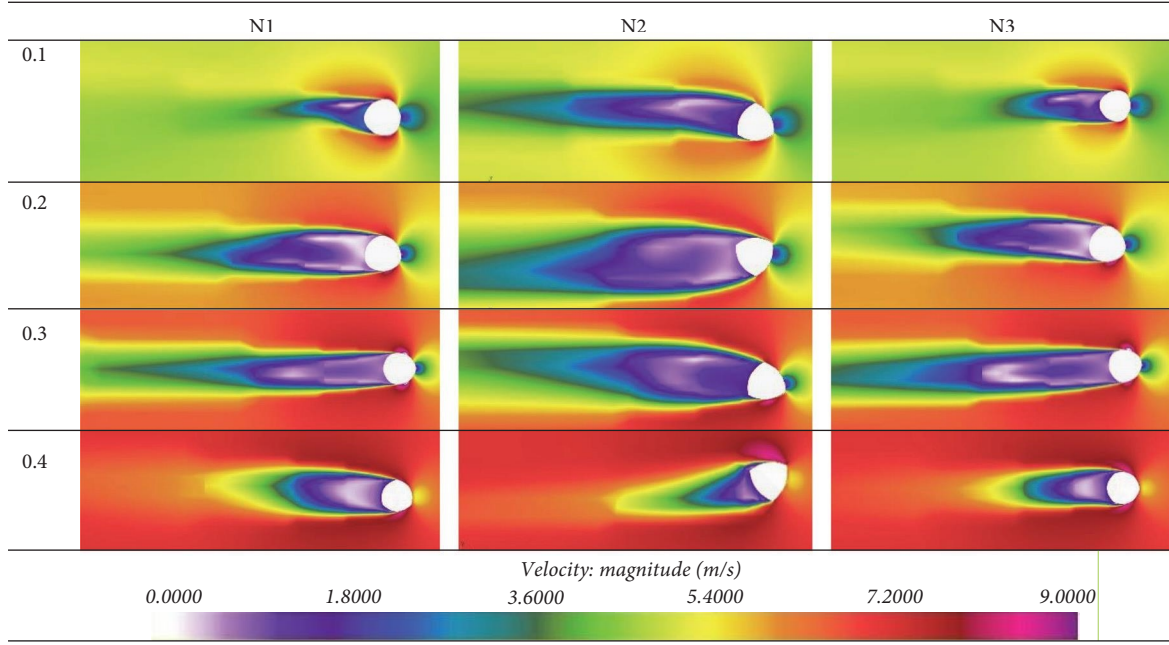
FIGURE 8: Velocity magnitude around the model from top view for three models and four different heights from ground bed.
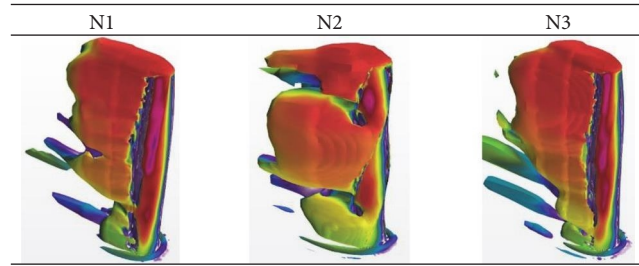

FIGURE 9: The Q-criterion parameter in three optimized models.

TABLE 1: Dimensional force, moment, and area.

Name	Rs (N)	Rp (N)	Rt (N)	Fy (N)	My (N.m)	Mz (N.m)	A (m^2)
N1	0.00829	0.2137	0.222	0.05798	0.04743	−0.00032	0.07134
N2	0.00695	0.3613	0.3682	−0.001	0.08012	0.000038	0.0788
N3	0.00853	0.2117	0.2203	0.008661	0.04665	−2.06E-05	0.07171

TABLE 2: Nondimensional force, moment, and area.

Name	C_F	C_P	C_t	C_{Fy}	C_{My}	C_{MZ}
N1	0.005105	0.131602	0.136713	0.0357056	0.073022	−0.00411
N2	0.003879	0.201426	0.205273	−0.000555	0.111668	0.000452
N3	0.005225	0.129698	0.134967	0.0053062	0.07145	−0.00026

around Y-axis coefficient and C_{Mz} is moment around Y-axis coefficient.

According to Tables 1 and 2, the least shear force is related to N2; also, the least pressure and total resistance are in or N3 model. Additionally, the least Z and Y moments are for the N3 model.

In conclusion, N3 is the best model based on the optimized aerodynamics concepts. Also, N3 model is better than the two ones in terms of aerodynamics approach. Low C_D, C_{My}, and C_{Mz}, as the most important parameters in aerodynamics analysis of the tall buildings, resulted in the most optimized shape of the model.

6. Conclusion

In this research, certainly, three triangle-optimized models were investigated by using the CFD method. Turbulence intensity and velocity profile were modeled by functions in STAR CCM+, and k-ε turbulent model was employed for calculating Reynolds restores. Also, RANS equations were used for flow momentum. For verification of the results, a solution was verified by 1.8E6 mesh grids, and scenario tests were running. The main results of this research are as follows:

(i) Surface in front of air for N2 is less than the two others, and result is more pressure. Also, drop pressure around the hull in N2 model is less than in two other models.

(ii) Separation of the airflow in N3 and N1 occurs later than in the N2 model, and this phenomenon has more eddy pressure consequences. Another important result is about N3 in comparison of N1, where the separation of the airflow happens later.

(iii) The middle of the N2 wake is so greater than the two other models. It can increase the pressure drag extremely. Also, the wake of the N3 back tower is less than the N1 model.

(iv) The least shear force is related to N2; also, the least pressure and total resistance are in or N3 model. Additionally, the least Z and Y moments are for the N3 model.

(v) In conclusion, N3 is the best model based on the optimized aerodynamics concepts.

Data Availability

Requests for access to these data should be made to the corresponding author email address: mehdi.noormohamadian@eng.uk.ac.ir.

Conflicts of Interest

The authors declare that they have no conflicts of interest.

References

[1] H. E. Dickson, "*The Chicago School of Architecture: A History of Commercial and Public Building in the Chicago Area, 1873–1925*. By Carl W. Condit. (Chicago: University of Chicago Press, 1964. xviii+ 238 pp. Illustrations, bibliography, and index. \$8.50.)," *Journal of American History*, vol. 52, no. 1, pp. 180-181, 1965.

[2] M. M. Ali and K. S. Moon, "Advances in structural systems for tall buildings: emerging developments for contemporary urban giants," *Buildings*, vol. 8, no. 8, Article ID 104, 2018.

[3] G. F. Menzies and J. R. Wherrett, "Multiglazed windows: potential for savings in energy, emissions and cost," *Building Services Engineering Research and Technology*, vol. 26, no. 3, pp. 249–258, 2005.

[4] P. A. Irwin, "Bluff body aerodynamics in wind engineering," *Journal of Wind Engineering and Industrial Aerodynamics*, vol. 96, no. 6–7, pp. 701–712, 2008.

[5] S. Lee and S. Hershberger, "A simple rule for generating equivalent models in covariance structure modeling," *Multivariate Behavioral Research*, vol. 25, no. 3, pp. 313–334, 1990.

[6] R. Irwin, "Negotiating feelings in the field: analyzing the Cultural Shock1," *Revista Brasileira de Sociologia da Emoção, GREM, UFPA*, vol. 8, no. 23, pp. 344–371, 2009.

[7] K. C. S. Kwok, M. D. Burton, and A. Abdelrazaq, "Wind-induced motion of tall buildings," *International Journal of High-Rise Buildings*, vol. 4, no. 1, pp. 1–8, 2015.

[8] S. M. S. Kolbadi, H. Piri, A. Keyhani, S. M. S. Kolbadi, and M. Mirtaheri, "Seismic performance evaluation of slotted-web and bolt-flange plate moment connection," *Earthquakes and Structures*, vol. 20, no. 6, pp. 655–667, 2021.

[9] S. M. S. Kolbadi, N. Hassani, S. M. Seyed-Kolbadi, and M. Mirtaheri, "Analyzing parametric sensitivity on the cyclic behavior of steel shear walls," *Shock and Vibration*, vol. 2021, Article ID 3976793, 10 pages, 2021.

[10] E. Bernardini, S. M. J. Spence, D. Wei, and A. Kareem, "Aerodynamic shape optimization of civil structures: a CFD-enabled Kriging-based approach," *Journal of Wind Engineering and Industrial Aerodynamics*, vol. 144, pp. 154–164, 2015.

[11] A. Elshaer, G. Bitsuamlak, and A. El Damatty, "Enhancing wind performance of tall buildings using corner aerodynamic optimization," *Engineering Structures*, vol. 136, pp. 133–148, 2017.

[12] M. Noormohamadian and E. Salajegheh, "Evaluation and minimization of moment coefficient of tall buildings with trilateral cross-section via a surrogate model," *SN Applied Sciences*, vol. 3, Article ID 234, 2021.

[13] N. Lin, C. Letchford, Y. Tamura, B. Liang, and O. Nakamura, "Characteristics of wind forces acting on tall buildings," *Journal of Wind Engineering and Industrial Aerodynamics*, vol. 93, no. 3, pp. 217–242, 2005.

[14] S. Kwok, "From red giants to planetary nebulae," *Astrophysical Journal*, vol. 258, pp. 280–288, 1982.

[15] H. Hayashida and Y. Iwasa, "Aerodynamic shape effects of tall building for vortex induced vibration," *Journal of Wind Engineering and Industrial Aerodynamics*, vol. 33, no. 1–2, pp. 237–242, 1990.

[16] P. Irwin, J. Kilpatrick, J. Robinson, and A. Frisque, "Wind and tall buildings: negatives and positives," *The Structural Design of Tall and Special Buildings*, vol. 17, no. 5, pp. 915–928, 2008.

[17] F. Miao, X.-J. Yang, L. Zhou et al., "Structural modification of sanguinarine and chelerythrine and their antibacterial activity," *Natural Product Research*, vol. 25, no. 9, pp. 863–875, 2011.

[18] Y. Kim and J. Kanda, "Characteristics of aerodynamic forces and pressures on square plan buildings with height variations," *Journal of Wind Engineering and Industrial Aerodynamics*, vol. 98, no. 8-9, pp. 449–465, 2010.

[19] Y. C. Kim and J. Kanda, "Wind pressures on tapered and setback tall buildings," *Journal of Fluids and Structures*, vol. 39, pp. 306–321, 2013.

[20] M. Noormohamadian and E. Salajegheh, "Multi-objective aerodynamic optimization of the exterior shape of tall buildings with trilateral cross-section," *Journal of Rehabilitation in Civil Engineering*, vol. 10, no. 4, pp. 129–145, 2022.